16th SYMPOSIUM OF THE IAHR
SECTION ON HYDRAULIC MACHINERY AND CAVITATION
SÃO PAULO / BRAZIL
14th to 18th SEPTEMBER 1992

EROSION AND IMPACT INTENSITY OF VIBRATORY, JET AND TURBINE CAVITATION

ÉROSION ET INTENSITÉ DES IMPACTS DE LA CAVITATION VIBRATOIRE, DE JET ET DES TURBINES

SIMONEAU, Raynald Ph.D. Hydro-Québec Canada
BOURDON, Paul Eng. Hydro-Québec Canada
IREQ, Varennes, J3X 1S1

SUMMARY

The ratio of the cavitation erosion resistance of the new austenitic stainless steel Hydroloy to the one of the standard 308 has been found to vary from 11 to 16 in vibratory cavitation tests to about 5 in large hydroturbines. Cavitation erosion tests in a high pressure water jet show also the same range of resistance ratio between 4 and 6 as in large turbines. It has been postulated that this behavior was related to the impact intensity of individual cavitation collapses and the deformation stress of these steels. To verify that hypothesis simultaneous erosion rate and impact intensity have been measured in vibratory and jet cavitation tests. An electrochemical titanium erosion detector coupled to a high frequency accelerometer is used. These measurements coupled with those of pit size distribution on aluminum confirm that the impact energy in jet cavitation can be more than two orders of magnitude larger than in the 20 kHz vibratory cavitation. The inferred forces of these impacts are then compared with those measured on a cavitation tunnel NACA profile, a turbine model and its prototype. It is concluded that vibratory cavitation produces mainly fatigue elastic deformation on higher resistance alloys whereas high velocity flow cavitation produces more plastic deformation and/or brittle fracture.

RÉSUMÉ

Le rapport de la résistance à l'érosion de cavitation du nouvel acier inoxydable austénitique Hydroloy à celle de l'acier inoxydable standard 308 varie de 11 à 16 dans l'essai de cavitation vibratoire à 5 environ dans les grandes turbines hydrauliques. On trouve la même gamme de rapport entre 4 et 6 dans des essais de cavitation au jet à haute vitesse. On a émis l'hypothèse que ce comportement était relié à l'intensité des impacts de cavitation et à la contrainte de déformation de ces aciers. Pour vérifier cette hypothèse on a mesuré, dans les essais vibratoires et au jet, le taux d'érosion et l'intensité des impacts simultanément à l'aide d'un détecteur d'érosion électrochimique en titane couplé à un accéléromètre à haute fréquence. Ces mesures couplées à celles des distributions de diamètres de marques d'impacts sur aluminium confirment que l'énergie des impacts de cavitation peut être plus de deux ordres de grandeur plus forte au jet que dans l'essai vibrant à 20 kHz. Les forces inferrées par ces impacts sont ensuite comparées à celles mesurées sur un profil NACA dans un tunnel à haute vitesse et sur des modèles et protoypes de turbines hydrauliques. On conclue que la cavitation vibratoire produit, sur les alliages à haute résistance, surtout des déformations élastiques de fatigue alors que la cavitation des écoulements à haute vitesse produit plus de déformation plastique et/ou de ruptures fragiles.

INTRODUCTION

The standard ASTM G32 vibratory cavitation test has been widely used to rank the cavitation erosion resistance of a large number of metals and industrial alloys. This test is fast and simple and has proved very useful in the choice of the best commercial alloys and also for the development of new alloys to fight cavitation erosion in large hydroturbines and pumps in the power industry. Results obtained in the last ten years at Hydro-Québec illustrate well that point[1]. A new high strain-hardening austenitic stainless steel has been de· loped and used for 4 years as welding wire under the trade name Hydroloy HQ 913 to repair the most severe cavitation damages in large hydroturbines[2-3-4]. This steel shows erosion rates 5 times lower than the one previously observed in these machines repaired with the standard 308 austenitic stainless steel[5].

These very good results have raised however an unanswered question: why is the erosion resistance ratio of Hydroloy to 308 only 5 on the average in the field whereas it is rather 13 in the standard vibratory test in the laboratory ? In an attempt to elucidate that puzzle a series of tests, including weight losses on three different materials, 6061 aluminum, 308 stainless steel and Hydroloy, as well as electrochemical and acoustic measurements, have been carried out in vibratory and jet cavitation. The measured cavitation impact forces will be compared with those measured on a NACA profile and on model and prototype hydroturbines.

THE RELATIVE CAVITATION EROSION RESISTANCE

To study the effect of the relative ratio of the impact stresses to the material deformation stresses a wide range of cavitation impact stress and of material yield stress was investigated. The 6061 aluminum alloy in the T6 temper condition with a hardness of 63 RB was used as a reference material. It does not show any deformation induced transformation as do the two austenitic stainless steels 308 and Hydroloy. These two steels have an as welded hardness of respectively 86 RB and 27 RC. The standard 20kHz vibratory test was used at three different peak-to-peak amplitudes, 25, 50 and 70μm. The collapse intensity was further increased by going to a cavitating jet operating at very high water velocity and producing higher erosion rates with a lower repeating frequency of cavitation impacts. This jet is produced by a 0.5 mm diameter sapphire nozzle submerged in tap water between 15 and 25 °C. The driving jet high pressure is varied between 7 and 41 MPa (6000 psi) and the ambient pressure of the test chamber between 0 and 0.41 MPa (60 psi).

Figures 1and 2 summarize the weight loss results plotted against the weight losses of 6061 aluminum alloy in the T6 temper taken as a reference material. The change of slope on figure 1 when going from vibratory to jet cavitation is indicative of a change of regime in the material erosion process. In particular for Hydroloy the jet linear regression line seems to indicate a threshold intensity at about 100 mg/h of Al. The cavitation resistance is defined as the inverse of the weight loss ratio. The ratio of the cavitation resistance of Hydroloy HQ 913 to that of 308 stainless steel decreases from 14 to 10 when the vibration amplitude increases from 25 μm to 70 μm. Under the cavitating jet this ratio decreases only marginally, from 5.3 to 4.6, when going from the lowest erosion rate to the maximum one.

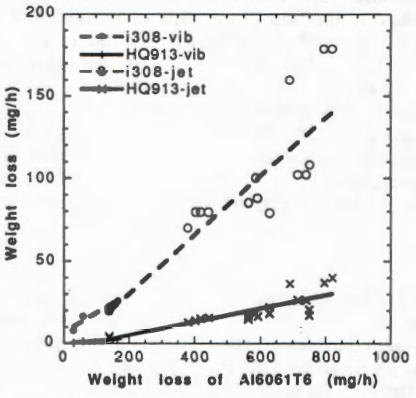

Fig.1 Weight losses in vibratory and jet cavitation tests.

The same range of resistance ratio is found in the jet tests as in large turbines. Figure 3 is an example of results obtained on a 200 Mw Francis runner repaired with both steels and inspected after two 20000 h operation periods. On the average for the 13 blades a cavitation resistance ratio of 5 is found. These results show that the cavitation jet offers a much better simulation of the cavitation occurring in large machines.

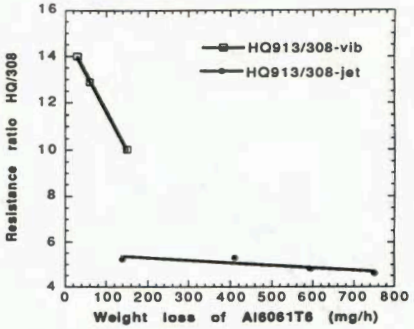

Fig. 2 Cavitation erosion weight loss ratio in the vibratory and jet tests.

VIBRATORY CHARACTERISTICS OF EROSION

In order to better correlate the impact intensity through its acoustic vibratory emission with the erosion process, a special sensor was designed integrating an electrochemical titanium erosion detector, DECER, and a high frequency accelerometer. The principles and methods used with these two types of sensors have been described in previous publications[6,7,8,9]. The 13 mm diameter titanium cylinder is maintained at a fixed electrochemical potential via a stainless steel reference electrode and a potentiostat. The current signal of the pre-incubated titanium probe is directly proportional to the metal weight loss rate, with a calibration factor of 0.05 mg/h per μA in vibratory cavitation. A miniature high frequency accelerometer is directly attached to the titanium cylinder; its mounted resonance frequency is measured at 125 kHz and its dynamic range is 10000 g peak-to-peak with a calibration factor of 0.789 mV/g. Its signal is analyzed with three different systems having frequency bandwidth of 20, 100 and 1000 kHz respectively. In order to infer excitation forces on the profile under cavitating conditions from measured acceleration values, the transmissibility function was measured in the 0-100 kHz frequency band by exciting the titanium surface with a miniature instrumented force hammer[9]. The titanium sensor surface was maintained stationary at 0.5 mm of the vibrating horn tip in the vibratory cavitation tests and at 5 mm of the 0.5 mm cavitation jet nozzle.

Figure 5 presents the results of the vibratory cavitation tests. The erosion rate of the titanium stationary specimen, as given by the DECER electrochemical current, is directly proportional to the vibration amplitude of the vibrating horn tip. The mean square value of the accelerometer output in the 0-20 kHz bandwidth does not correlate as well. As shown on

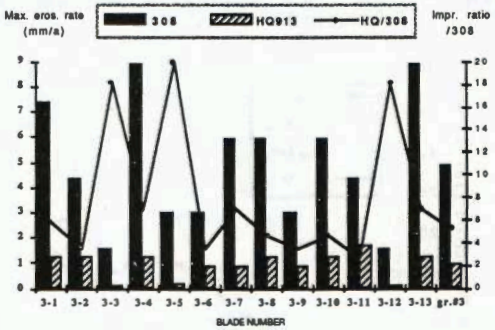

Fig. 3 Erosion rate measured on the 13 blades of a Francis runner repaired with 308 and Hydroloy.

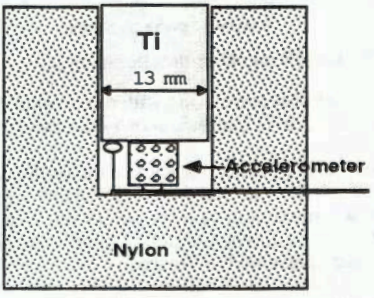

Fig. 4. The combined electrochemical acoustic DECER sensor.

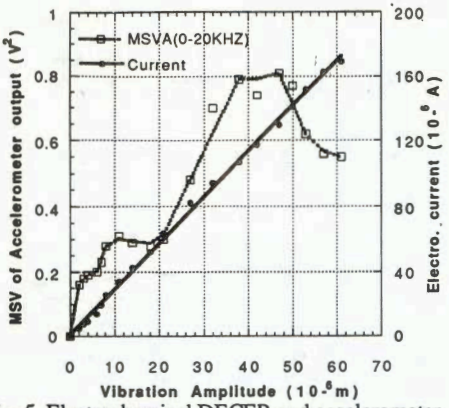

Fig. 5. Electrochemical DECER and accelerometer signals in the vibratory tests.

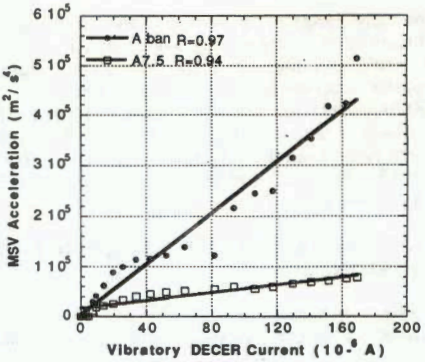

Fig. 6. MSV of acceleration in the 0.5-7.5 kHz bandwidth and in the corresponding sidebands vs vibratory cavitation erosion DECER current.

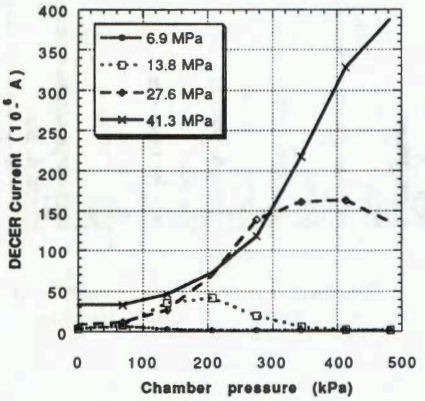

Fig. 7 DECER signal in the cavitating jet.

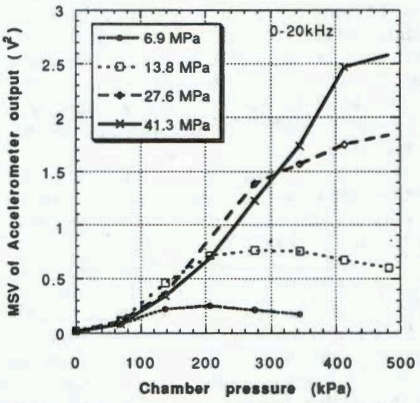

Fig. 8. Accelerometer signal in the cavitating jet.

figure 6 the best correlation with the erosion rate was found for the mean square value of acceleration in the 0.5-7.5 kHz bandwidth or in the two first side bands around the 20 kHz fundamental excitation frequency.

Figures 7 and 8 present the same data for the cavitating jet tests. Here again the correlation between the DECER erosion rate and the accelerometer signal is not perfect. As an example the acceleration data do not show a maximum as it should for the 27.6 MPa high pressure case. Here too a better correlation is found with the lower frequency bandwidth 0.5-11kHz, as illustrated on figures 9 and 10. The two autospectra presented on figures 11 and 12 show indeed that the effect of erosion is mostly reflected in the 0.5-7.5 kHz band and the 19 kHz sidebands for the vibratory cavitation and in the 0.5-11 kHz band for the jet cavitation.

For vibratory cavitation the peak in the 2.5 kHz region shifts towards lower frequency as the cavitation intensity increases. This peak, corresponding to higher intensity impacts as we can see on the time

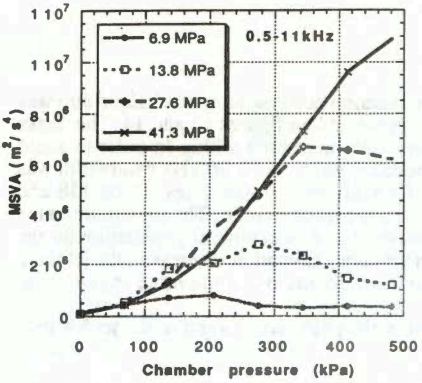

Fig. 9 MSV of 0.5-11 kHz acceleration in jet cavitation.

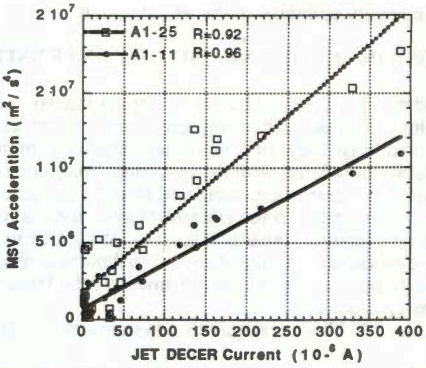

Fig.10 MSV of acceleration in the 0.5-11 and 0.5-25 kHz bands vs jet erosion DECER current.

charts of figures 13 and 14, could be attributed to the coherent collapse of a group of bubbles or of a cavity cluster[10]. The volume of this cavitation cloud grows with the cavitation intensity and its collapse frequency decreases accordingly. On the time spectrum of figure 14 we can see the 125 kHz resonance of the accelerometer being excited not only for the largest impacts but also on one polarity of the 20 kHz oscillations, corresponding to the position of the smallest gap at 20 kHz between the accelerometer mounting surface and the vibrating horn tip. These excitations are attributed to bubble or smaller cavity cluster collapses on every positive pressure cycle produced by the vibrating tip. These smaller impacts are much more numerous than the larger ones and contribute largely to the erosion process.

Inversely for the jet cavitation, as seen on figure 12, the low frequency peaks shift towards higher frequency as cavitation increases. This should be attributed to the higher water velocity producing higher erosion rates according to a Strouhal law. This modulation is well illustrated on the time spectrum of figure 13. On figure 14 we see no excitation between the

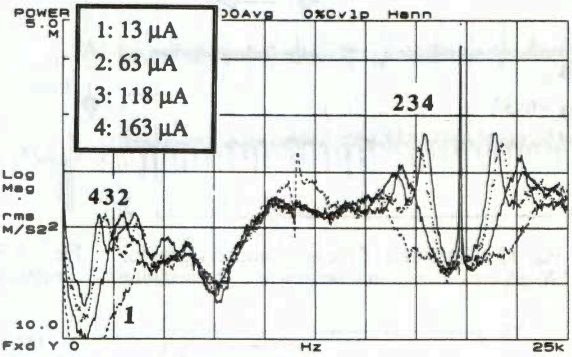

Fig. 11 Accele. autospectra for the vibratory cavitation.

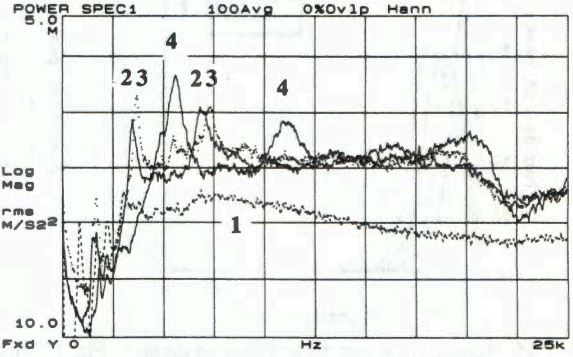

Fig.12. Acceleration autospectra for the jet cavitation.

high intensity collapses of the jet cavitation.

EROSION RATE AND IMPACT INTENSITY

In order to get the distribution of impact intensities of the cavitation collapses a special algorithm was developed to calculate histograms from time traces such as presented on figures 13 and 14. The peaks are considered only for a minimum threshold intensity and a minimum peak width. In order to avoid the peaks associated with the resonance frequency of the accelerometer, the 0-20 kHz bandwidth was chosen. Histograms are calculated from 85 ms time scans of 4 equivalent erosion rates (11-68-118-and 163 μA) on figure 15 for vibratory cavitation and on figure 16 for jet cavitation. The maximum value of the acceleration signal is at least twice as large in jet cavitation than it is in vibratory cavitation for the same erosion rate. A nice normal distribution is observed in vibratory cavitation whereas in the jet there seems to be two populations of impacts, the large intensity ones getting more and more important at higher erosion rates.
With the 20 kHz data acquisition system not only the height of the peaks were larger in the jet but they

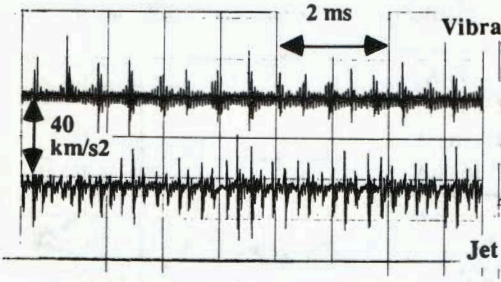

Fig. 13. Time chart of the acceleration signal for 120 μA erosion rate in vibratory and jet cavitation.

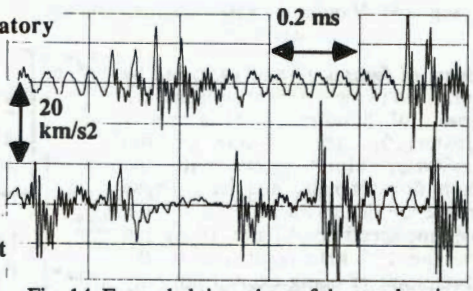

Fig. 14. Expanded time chart of the acceleration signal for 120 μA erosion rate as on fig. 13.

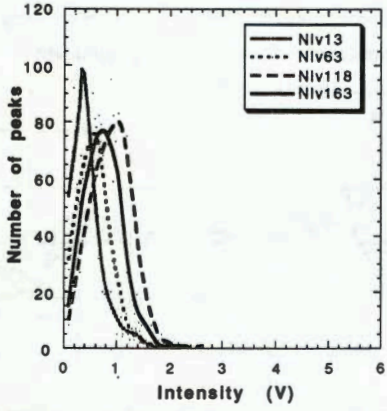

Fig. 15. Histogram of vibratory cavitation impact intensity for 4 erosion rates.

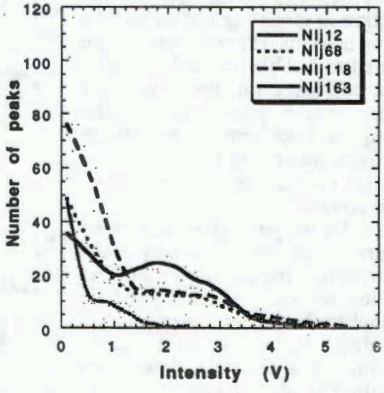

Fig. 16. Histogram of jet cavitation impact intensity for 4 erosion rates.

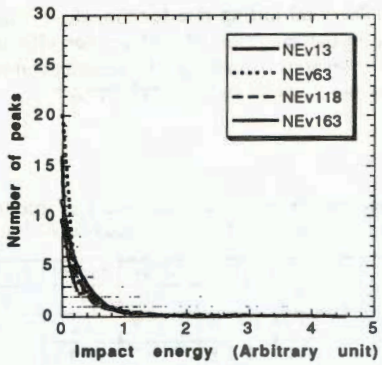

Fig. 17. Histogram of vibratory cavitation impact energy for 4 erosion rates.

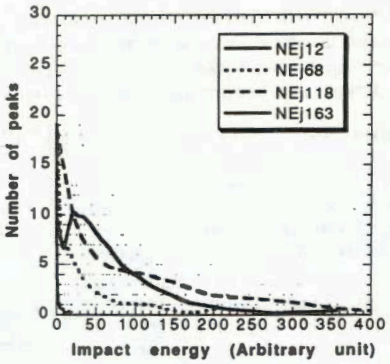

Fig. 18. Histogram of jet cavitation impact energy for 4 erosion rates.

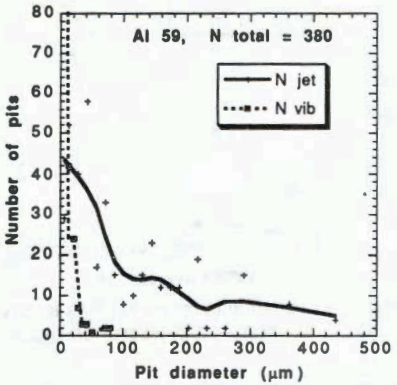

Fig. 19 Histogram of pit diameter produced on soft pure Al by vibratory and jet cavitation.

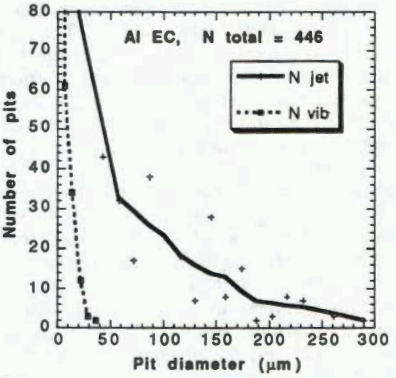

Fig. 20 Histogram of pit diameter produced on EC aluminum by vibratory and jet cavitation.

were also wider since the 125 kHz resonance was not resolved. To have a better evaluation of the energy of the impacts the area under the peaks (amplitude vs time) was integrated. The energy of the cavitation impacts is proportional to the square of these area values. The results are shown on figures 17 and 18. For the same erosion rates the impact energies of the jet cavitation impacts are more than two orders of magnitude larger than those of vibratory cavitation impacts.

To validate these data the diameters of pits indented on soft pure aluminum 59 (hardness BHN 15) and Electrical Grade aluminum (BHN 57) by 3 seconds of cavitation impacts both in vibratory and jet cavitation at equivalent erosion rate of 170 μA of DECER current were measured. As shown on figures 19 and 20 most of the vibratory cavitation pits are within the 5 to 20 μm range whereas the diameters of jet cavitation pits are distributed from 10 to 400 μm. For both aluminum alloys the cavitation pit distribution is very similar to the impact energy distribution given by the accelerometer. Since the deformation energy should be proportional to the square or even the cube of the pit diameter, these pit measurements confirm that the average energy of the jet cavitation impacts is at least two orders of

magnitude larger than the vibratory cavitation impacts. The total pitting rate for the whole eroded surface area was estimated from these pit counts to be in the range of 40 000 s^{-1} for vibratory cavitation and around 1000 s^{-1} for jet cavitation. Even if it is obvious that all the pits were not counted, these pitting rates confirm the higher vibratory impact frequency detected by the accelerometer.

COMPARISON WITH FLOW CAVITATION

In order to compare these impact intensity measurements with the cavitation impacts of large hydroturbines we have to use the inferred force deduced from the measured acceleration and the transmissibility function. These inferred forces and transmissibility functions together have been measured with the same instrumented hammer technique in the five different cavitation set-ups listed in table 1, in vibratory and jet cavitation, on a 150X100 mm^2 NACA profile in a high speed cavitation tunnel [9] and on a model (1/13 scale) and a prototype of a 33 MW Francis turbine. The frequency bands of the inferred forces, shown in table 1, are the ones where most of the measurable erosive energy was concentrated for each set-up. To correlate with the local erosion rate the mean square value of the inferred force is applied to the surface area showing cavitation erosion. On the 15 blade Francis turbines the MSV of inferred force per blade is considered at the operating point (75 % wicket gate opening) where the prototype was operated for 80 % of its 18000 hour exposure period. On the prototype the maximum local erosion rate is given by the field inspection value of 0.7 mm/a of 308 stainless steel which is equivalent to 3.6 mm/a of titanium grade 2, the DECER probe material [11,12] and the observed damaged area.

Table 1. Eroded surface area, maximum MSV of inferred force and maximum erosion rate for various cavitation.

	vib.	jet	NACA	model	proto.
Surface (cm^2)	1.8	1	150	1	180
F^2max (N^2)	1314	2.10^4	5.10^5	10	3.10^6
Frequen.(kHz)	1-62	.5-25	.06-3	.5-10	1-11
E.R. (mm/a Ti)	90	387	1	0.01	3.6

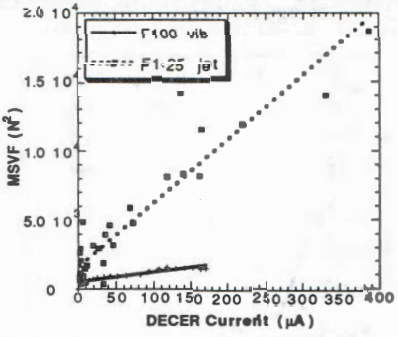

Fig 21. Correlation between MSV of inferred force and vibratory and jet erosion signal.

The erosion rate of the model was deduced from previous measurements indicating erosion rates on a model tested in equivalent conditions to be 300 times less than on the prototype [11] and from the attack areas on the blades revealed by pressure tapes.

The inferred forces are the only measure that can be really compared from one set-up to the other. In view of the different mass, stiffness and damping distribution of each determining the vibratory response of that structure to a given excitation, it is essential to analyze each situation individually and to determine from the measured acceleration response spectra which portion is related to erosive cavitation excitation as opposed to other excitation forces which may be present.

As has been observed in figures 6 and 10, good linear relations between MSV of acceleration and erosion can be obtained by selecting frequency bands where the acceleration response is clearly associated with cavitation excitation. Similarly, by the same procedure, good linear relations can be obtained as shown on figure 21 when the inferred forces are considered.

However, when comparing the results of one set-up with those of others, it becomes necessary to compare averaged inferred forces which have been produced by different hydrodynamic mechanisms in each set-up. In a given set-up some of these mechanisms generate overlapping response frequency spectra. As examples, the vibratory set-up produces both liquid pressure wave harmonic excitation and

impulsive excitation by imploding bubbles at 20 kHz. The water jet produces periodic cavitation impulses on the structure with a broad frequency content but so does the impinging jet flow on the target. In the high speed cavitation tunnel and on the model and the prototype, the basic flow noise associated with the surface roughness and cavitation implosions in the flow away from the structure also produce broad band excitation of the blades as do the imploding vortices and bubbles that attack directly the structure surface.

With these considerations in mind we present on figure 22 the correlation between erosion rates and inferred forces per unit area of attacked surface. For vibratory cavitation the total effective erosive forces lie between curve A showing forces that can only be explained by cavitation implosions and curve B showing the total inferred forces in the 1 - 62 kHz frequency band where meaningful values were measured.

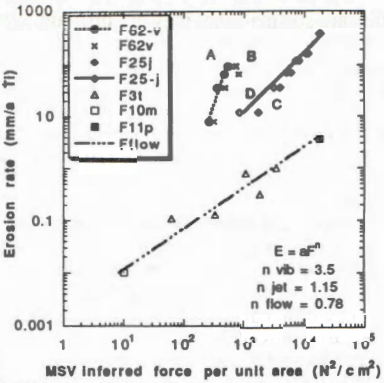

Fig. 22. Correlation between erosion rate and inferred force in all types of cavitation.

Curve C for the cavitating jet overestimates the forces attributable to cavitation implosions only since it includes the contribution of the jet flow impinging on the eroded target. This contribution is most significant at low erosion rates and flow velocities. Curve D was built by subtracting this contribution estimated from the lowest erosion rate measurements in the 0.5 - 25 kHz band. It delimits the region of inferred forces attributable to jet cavitation implosions on the surface.

The curve derived from measurements on the NACA profile in the cavitation tunnel also overestimates the forces involved in producing the measured erosion levels since it includes the contributions of the forces induced by the flow noise and cavitation implosions in the flow away from the profile. Similarly in a typical model test, responses due to flow noise in a cavitation free condition have been found to be about one order of magnitude smaller than the total response of the runner under cavitating conditions for practical wicket gate openings of 65 to 100 %. This ratio might be larger on a full scale prototype where typical surface roughness and velocities are greater than on small scale models. These considerations suggest that all the flow cavitation data points, for the NACA profile, the model and the prototype Francis turbines, should be shifted left by at least 10 % to better characterize the true inferred erosion forces.

The trends in the five data sets nevertheless indicate that higher inferred forces are involved for a given erosion rate as we move from the vibratory set-up, to the jet and then to the NACA profile and the Francis turbines. This is associated with an increase in individual impact intensities found in the three flow cavitation equipment which fall quite nicely on the same regression line. These trends reveal the relative erosion efficiency of each equipment, suggesting in particular that were significant flows are involved (tunnel, model and prototype) the large cavitation impacts and associated pressure fluctuations contribute more relatively to producing vibration of these structures rather than their erosion. This is not too surprising in view of the purpose of the various equipment! The trends also underline the need to better identify in each machinery those components of the vibratory response of a structure uniquely related to the cavitation impact process.

CONCLUSION

In all these flow cavitation experiments large acceleration crest factors have been found and indicate that high impact intensities are present wherever high mean square values of inferred forces are measured. The large pit diameters observed on the stainless steel of the NACA profile and of the prototype turbines also confirm the much higher impact intensities than in vibratory cavitation. Although some plastic deformation is visible on the 308 stainless steel surface in vibratory cavitation,

the pits are so small that they are difficult to identify. It is even more the case for the hardened surface of Hydroloy where during the long incubation period the surface remains quite flat with only some diffused plastic deformation. These observations indicate that in vibratory cavitation the lower energies of the erosive impacts stress the higher resistance alloys mainly in the elastic fatigue regime whereas the higher energy impacts of the jet and turbine cavitation cause more pronounced plastic deformation with ductile tearing and/or brittle fracture of the hardened layer. These different deformation behaviors can explain the lower resistance ratio of Hydroloy to 308 stainless steel in jet and turbine cavitation. This resistance ratio should be correlated with fatigue properties measured at different deformation amplitudes.

The experimental results presented lead to the following conclusions:

1. Jet cavitation produces much larger impact intensity and energy than vibratory cavitation.
2. The cavitation pit diameter distributions correlate well with accelerometer peak energy histograms.
3. This impact energy distribution affects the deformation and erosion behavior of industrial alloys.
4. Jet cavitation appears to better simulate hydroturbine cavitation.
5. The transmissibility function technique with high frequency accelerometer and instrumented hammer allows relative comparison of various cavitation erosion set-ups. However the hydrodynamics particularities of each situation must be analyzed carefully along with the mechanical characteristics of each set-up. Improvements in the method are required in the identification of structural responses exclusively attributable to cavitation erosion impulsive excitation.

ACKNOWLEDGMENT

The authors are grateful to Jacques Larouche and Pierre Lavigne for their skillful experimental work and dedicated collaboration.

REFERENCES

1 Simoneau, R., 1984. The optimum protection of hydraulic turbines against cavitation erosion. Proc. IAHR Symposium, Stirling, U.K. September 1984.

2 Simoneau, R., 1986. A new class of high strain-hardening austenitic stainless steels to fight cavitation erosion. Proc. IAHR Symposium, Montreal, Canada, September 1986.

3 Simoneau, R., Lambert, P., Simoneau, M., Dickson, J.I., L'Espérance, G., 1987. Cavitation erosion and deformation mechanisms of Ni and Co austenitic stainless steels. Proc. 7th. Conf. on Erosion by Liquid and Solid Impact, Cambridge, U.K. september 1987

4 Simoneau, R., Mossoba, Y., 1988, Field experience with ultra-high cavitation resistance alloys in Francis turbine. Proc. IAHR Symposium, Trondheim, Norway, June 1988.

5 Simoneau, R., Vibratory, Jet and Hydroturbine Cavitation Erosion, Cavitation and Multiphase Flow Forum of the First Joint ASME - JSME Fluids Engineering Conference, June 23-26, 1991, Portland, Oregon.

6 Simoneau, R., Fihey, J.L., Chincholle, L.,"Effet d'Activation Anodique de la Cavitation Érosive", Proc. 11th IARH Symposium , September 1982, Amsterdam (NL)

7 Simoneau, R., Désy, N., Grenier, R., "Electrochemical detection of cavitation erosion on a pump-turbine model", Proc. 13th IAHR Symposium, September 1986, Montréal (Canada).

8 Simoneau, R., Avellan, F., Kuhn de Chizelle, Y., "On line measurement of cavitation erosion rate on a 2D NACA profile" Proc. of Third International Symposium on Cavitation Noise and Erosion in Fluid System, ASME, December 1989, San Francisco (USA).

9 Bourdon, P., Simoneau, R., Avellan, F., Farhat, M., "Vibratory characteristics of erosive cavitation vortices downstream of a fixed leading edge cavity", Proc. 15th IARH Symposium, 11-14 September 1990, Belgrade (Yugoslavia).

10 Hansson, I., Morch, K. A., "Dynamics of cavity clusters in ultrasonic (vibratory) cavitation erosion", Journal of Applied Physics v 51 n 9, Sep. 1980.

11 Simoneau R., Bourdon, P., Désy N., Grenier R., "Cavitation detection in model tests of Hydraulic turbines, Phase 3 and Final Report", Canadian Electrical Association project 230G 439, 1988.

12 Bourdon, P., Simoneau, R., Lavigne, P., "A vibratory approach to the detection of erosive cavitation", Proc. of Third International Symposium on Cavitation Noise and Erosion in Fluid System, ASME, December 1989, San Francisco (USA).